Bedout: A Possible End-Permian Impact Crater Offshore of Northwestern Australia

L. Becker,[1]* R. J. Poreda,[2] A. R. Basu,[2] K. O. Pope,[3] T. M. Harrison,[4] C. Nicholson,[1] R. Iasky[5]

The Bedout High, located on the northwestern continental margin of Australia, has emerged as a prime candidate for an end-Permian impact structure. Seismic imaging, gravity data, and the identification of melt rocks and impact breccias from drill cores located on top of Bedout are consistent with the presence of a buried impact crater. The impact breccias contain nearly pure silica glass (SiO_2), fractured and shock-melted plagioclases, and spherulitic glass. The distribution of glass and shocked minerals over hundreds of meters of core material implies that a melt sheet is present. Available gravity and seismic data suggest that the Bedout High represents the central uplift of a crater similar in size to Chicxulub. A plagioclase separate from the Lagrange-1 exploration well has an Ar/Ar age of 250.1 ± 4.5 million years. The location, size, and age of the Bedout crater can account for reported occurrences of impact debris in Permian-Triassic boundary sediments worldwide.

The cause of the catastrophic mass extinction at the end of the Permian has been the focus of considerable debate. Becker *et al.* (*1*–*3*) and others (*4*–*10*) have presented evidence that a major impact was associated with the extinction of >90% of marine taxa. The evidence includes fullerenes with extraterrestrial helium and argon (*1*, *7*), meteorite fragments (*8*), Fe-Ni-Si "metamorphosed grains" of probable meteoritic origin (*5*, *8*, *9*), Fe-Ni metals with impact spherules (*6*, *10*), and shocked quartz (*4*).

Acceptance of the idea that an impact accompanied the Cretaceous-Tertiary (K-T) extinction increased dramatically with the discovery of the Chicxulub crater (*11*, *12*). We searched for a Permian-Triassic (P-T) boundary impact crater in parts of the Southern Hemisphere that once comprised the supercontinent of Gondwana, because the impact evidence is most abundant in continents from this region (such as Australia and Antarctica). Gorter, based on the study of a single seismic line (*13*, *14*), suggested that the Bedout ("Bedoo") High offshore of northwestern Australia might be the central uplift of a large end-Permian impact crater. In this paper, we describe the Bedout structure and present evidence from drill cores, additional seismic and gravity data, and Ar/Ar dating of plagioclases that Bedout is a large, buried, end-Permian impact crater and possibly the source of the P-T ejecta deposits distributed globally (Fig. 1 and fig. S1).

Geology of the Bedout structure. The Bedout High is part of the Roebuck basin, which forms the northwestern continental margin of Australia (Fig. 2). Existing studies of the structure include two regional seismic surveys conducted by the Australian Geological Survey (AGSO) and the Japan National Oil Company (JNOC) (*15*) and two exploratory wells drilled 9 km apart on the top and flank of the Bedout High (Bedout-1 and Lagrange-1) that extend to depths of 3052 m (9986 feet) and 3273 m (10,738 feet), respectively (Fig. 3 and fig. S2). Both wells were drilled through ~3 km of marine and fluvial sediments consisting of carbonates with occasional interbeded siltstones and mudstones (Tertiary to Cretaceous) and sandstones interbeded with claystones, siltstones, and coal (Cretaceous to Triassic) before reaching a breccia [Late Permian (fig. S2) (*16*)]. Two of the 14 AGSO regional seismic lines cross over the Bedout High (Fig. 2). In addition, four wells penetrate Permian strata (two are shown in Fig. 2) offshore that help to identify seismic reflectors that define the Bedout structure and stratigraphy. In both the Lagrange-1 and Bedout-1 cores and cuttings, fluviatile and marine Keraudren (Middle to Late Triassic) sediments are deposited directly on top of the breccia [Late Permian (Fig. 4 and figs. S2 and S3)].

Presently, the Bedout High stands several kilometers above the surrounding basement (*17*). Deep crustal reflections and seismic refraction velocities also suggest that the

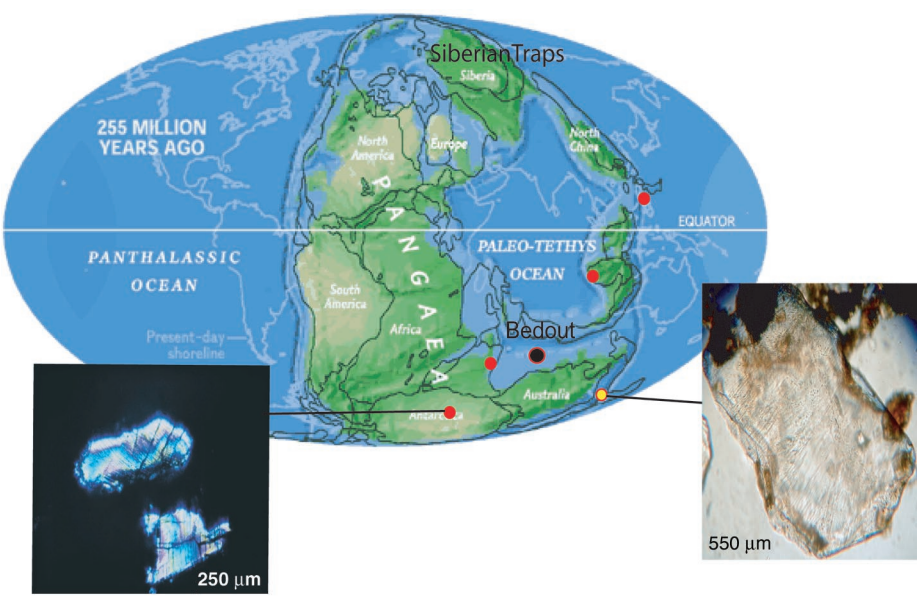

Fig. 1. Positions of the continents during end-Permian time. Red dots denote where extraterrestrial fullerenes have been reported. In addition, other suggested impact tracers have been found in P-T boundary layers at Graphite Peak, Antarctica; Meishan, China; and Sasayama, Japan, including meteoritic debris (*8*), Fe-Ni-Si grains (*5*, *8*), shocked quartz (*4*), and impact spherules (*6*). Recently, large shocked quartz grains (fig. S1) were found in the Fraser Park, Australia, and Graphite Peak, Antarctica, P-T boundary layer (yellow dot). [The Permian map was modified from the Scotese Paleomap Project Web site (www.scotese.com).]

[1]Institute for Crustal Studies, Department of Geological Sciences, University of California, Santa Barbara, CA 93106, USA. [2]Department of Earth and Environmental Sciences, University of Rochester, Rochester, NY 14627, USA. [3]Geo Eco Arc Research, Aquasco, MD 20608. [4]Australian National University, Canberra, Australia. [5]Geological Survey Western Australia, Perth, Australia.

*To whom correspondence should be addressed. E-mail: lbecker@crustal.ucsb.edu. Web page: http://beckeraustralia.ucsb.edu

Bedout High is underpinned by elevated middle and lower crust. Both core and cuttings cataloged as basalts and referred to as a "volcanic breccia" were recovered from the top of the High. This regional "volcanism" associated with rifting of the continental margin of Australia is classified as the "Bedout Movement" of P-T age (*18*, *19*). Immediately after the formation of the Bedout High and termination of the Bedout Movement, there is a regional angular unconformity at the top of the High, consistent with uplift and erosion at the end of the Permian (*20*). Coincident with the formation of the Bedout High is the rifting of the continental "Sibumasu sliver" off northeastern Gondwana (*21*). The resulting post-impact tectonism, uplift, faulting, and erosion during the Triassic and Jurassic time periods regionally overprinted the Bedout structure and deformed the original complex crater morphology.

The Bedout breccia. Both the Lagrange-1 and Bedout-1 exploration wells ended in what was inferred to be a volcanic breccia. Fifty-two meters—30 m of cuttings and 22 m of core—were collected from the breccia unit in Bedout-1, and 391 m of cuttings were sampled from the breccia unit in the Lagrange-1 drill hole. The Bedout core displays a series of centimeter-sized green clasts, some with variable banding and others that are poorly sorted (with chaotic dips of 30° to 50° in hand specimens) (Fig. 4 and fig. S3) over the entire core length (*20*). Most of the clasts throughout the core are dark green and massive and appear glassy in hand specimens, but in thin section many are partially altered to fine-grained chlorite or a mixture of fine-grained plagioclase, carbonate, and Fe oxides**.** We identified unaltered glass and relic igneous mineral grains from the lowest section of the core, at 3044 m (9986 feet) (Figs. 5 to 8 and figs. S4 to S14). A section from higher in the core at 3041 m (9977 feet) also contains several large and highly fractured plagioclase phenocrysts (figs. S8 and S9). The basal 8 m of the core contains many small rock and mineral clasts in a predominately glassy matrix that has partially altered to chlorite. Brownish glass shows evidence of flow structure (fig. S10), and calcite is observed as veins and in cavities in several thin sections (figs. S11, S13, and S14). The mineral clasts are mostly single and multiple aggregates of plagioclase, and the lithic clasts are of glassy fragments. The complex mixtures and very different textures in the lower 8 m of the core are similar to the cores from inside the Chicxulub crater (*22*–*25*) (Fig. 4 and figs. S3, S9, and S10 to S14).

The clast from 3044 m (9986 feet) contains shocked minerals surrounded by a matrix that is almost entirely glass, except where it has been altered to chlorite. The samples include shock-melted plagioclase that has been completely or partially converted to glass (Figs. 6 and 8), spherulitic glass (Fig. 7, A and B), and pure silica glass (SiO_2) (Fig. 7C). Plagioclase encloses diaplectic glass (maskelynite) with a composition identical to that of the surrounding plagioclase anorthosite (An_{50}) (Fig. 8, analyses 3 and 4 in table S1). We also identified magnesian iron titanium oxide [$(Fe_{.84}, Mg_{.14})\ TiO_3$]

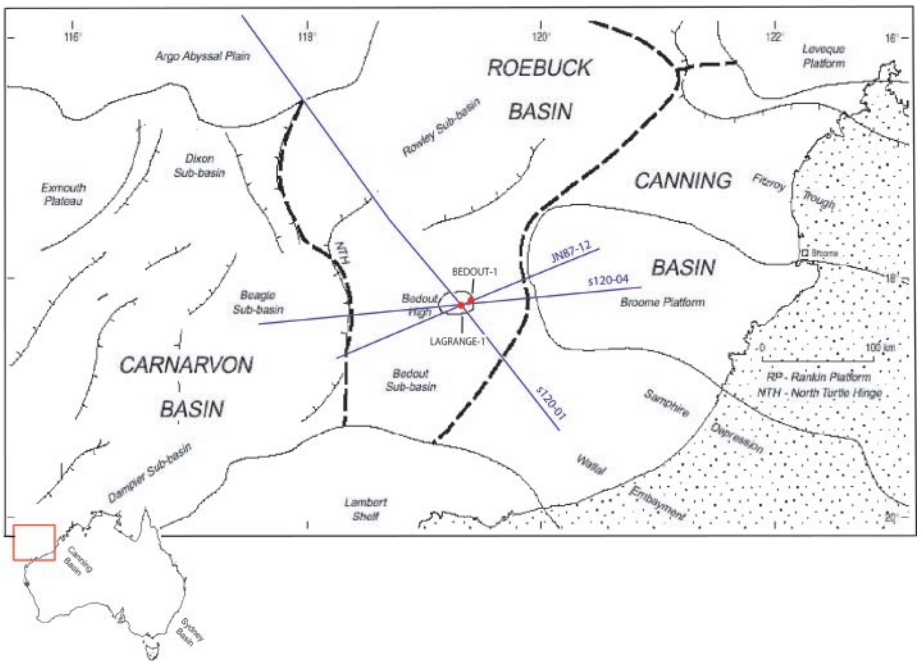

Fig. 2. Base map of the offshore northwestern Canning basin region, showing major tectonic elements such as plateaus, basins, and platforms;, the Bedout High with the Lagrange-1 and Bedout-1 exploration wells located on top of the high (red dots); and two AGSO regional seismic reflection lines (Figs. 3 and 10 and fig. S16) and the JNOC (JN87-12) seismic line (Fig. 3) that cross over the High [base map modified from (*17*)].

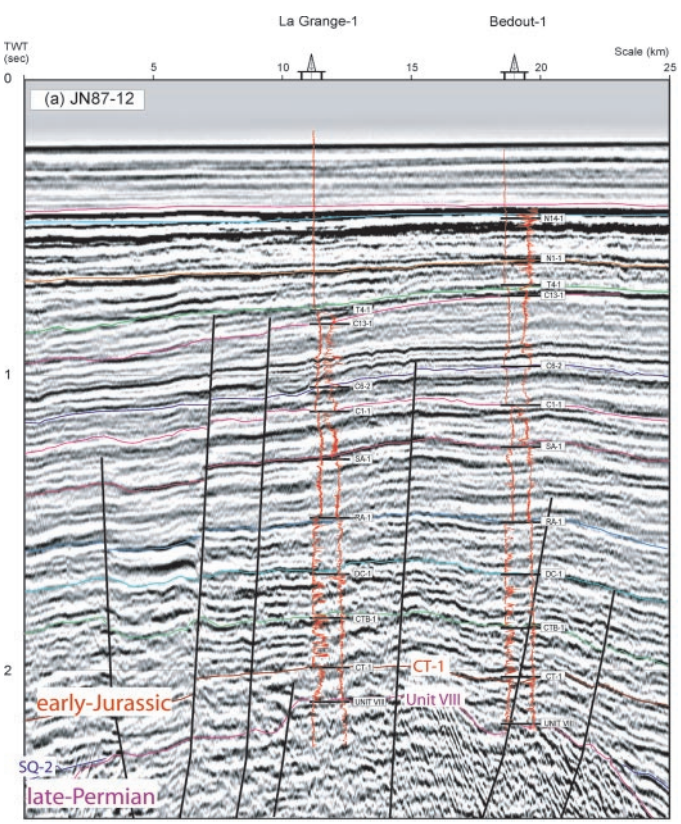

Fig. 3. Interpreted section of the multichannel seismic line JN87-12, showing correlated ties to Bedout-1 and Lagrange-1 gamma (**left**) and sonic (**right**) well logs [modified from (*16*); the location of the line is shown in Fig. 2]. Color stratigraphic horizons represent chronostratigraphic picks (CT-1, early Jurassic, red; SQ-2, middle Triassic, blue; Unit VIII, late Permian, purple). Triassic sedimentary rocks overlying the Upper Permian (unit VIII) are thin; however, all of the units were identified in the Bedout-1 and Lagrange-1 cores and cuttings (fig. S2).

grains that are stoichiometrically ilmenite, heterogeneous silica glass, albite, sanidine, and a partially melted carbonate ($CaCO_3$) clast with fragmented ooids (*26*, *27*) (Figs. 5 to 8 and figs. S4 to S7, A and B; table S1). Sanidine, identified optically and confirmed by microprobe analysis of a 10-μm grain (analysis 5 in table S1), has 43% albite in solid solution without any sign of segregation (microperthite).

The Lagrange-1 cuttings consist of various types of partly crystalline and partly glassy rock of mostly basaltic composition (fig. S7). Some of the fragments are identical to those found in the Bedout core (figs. S11 to S15). One of these fragments, from 3255 m (10,679 feet), is shown in fig. S7, A and B. fig. S7A shows feldspar crystallites (laths) in "swallowtail" terminations, indicating rapid crystallization from the glassy matrix. The feldspar laths display heterogeneous compositions and are mixtures of either pure albite (table S2, no. 1) or K-feldspar (table S2, no. 2) in their glassy matrix (table S2, no. 3), as seen in the backscattered image (fig. S7B) of one of the grains.

We interpret these textures, chemistry, mineralogy, and mixture of different fragments as indicating that the basal 8 m of Bedout-1 is an impact melt breccia. The completely or partially melted and fractured plagioclase crystals and abundant glassy clasts are most diagnostic. The coexistence of titanium-rich silica glass in close proximity (within 1 mm) to titanium-poor but slightly aluminous silica glass (analyses 23 and 24 in table S1 and Fig. 7C) requires silicate liquid immiscibility that is not seen in terrestrial magmatic environments.

Partially melted and recrystallized carbonate lithic fragments (Fig. 5) and spherulitic glasses (partially altered to chlorite; Fig. 7B and analysis 22 in table S1), with a different chemical composition from the glassy matrix, are again features attributable to an impact-generated melt breccia. Magnesian-ilmenite (analysis 20 in table S1) found as microlites in the matrix is also an uncommon mineral in volcanic rocks. The glassy rock clasts can be attributed to the melting of target materials that contained Mg-rich sediments (such as dolomites) and common Fe-Ti oxides (such as magnetite, titanite "sphene," and rutile), which are found in crustal environments. Overall, the compositions of the minerals

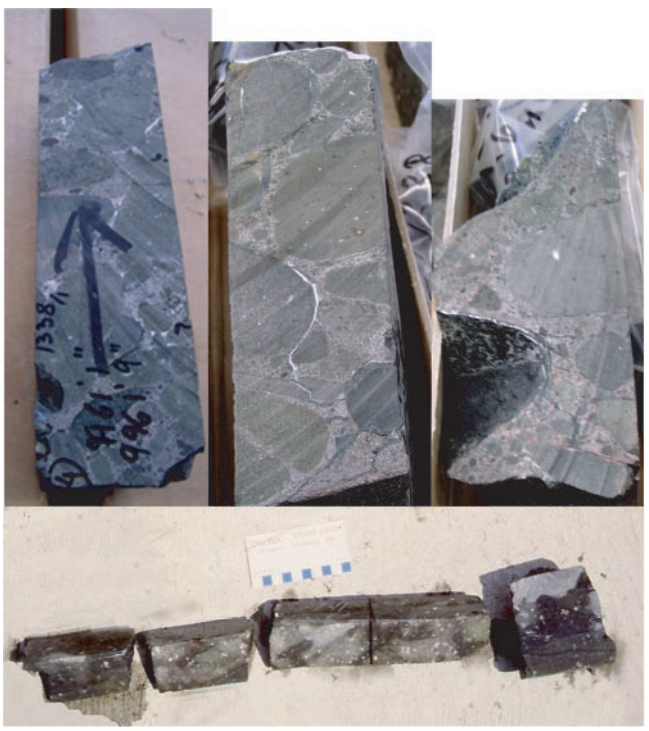

Fig. 4. Selected, intact, 5-cm-wide core from Bedout-1 at 3035 to 3037 m (9960 to 9965 feet; top three photos). These cores display variable-sized, angular, and subrounded glassy (impact-melted) fragments set in a matrix that is mostly chloritized and carbonate-filled. The smaller glassy fragments examined in thin section throughout the core (figs. S8 to S14) displayed the same mineralogy and texture as the larger impact-melted glassy fragments seen in hand specimens. The lower photo is the Yucatan-6 impact melt breccia, which has similar characteristics to the Bedout-1 specimens, particularly in hand specimens (the Yucatan-6 core photo was modified from www.icdp-online.de/.

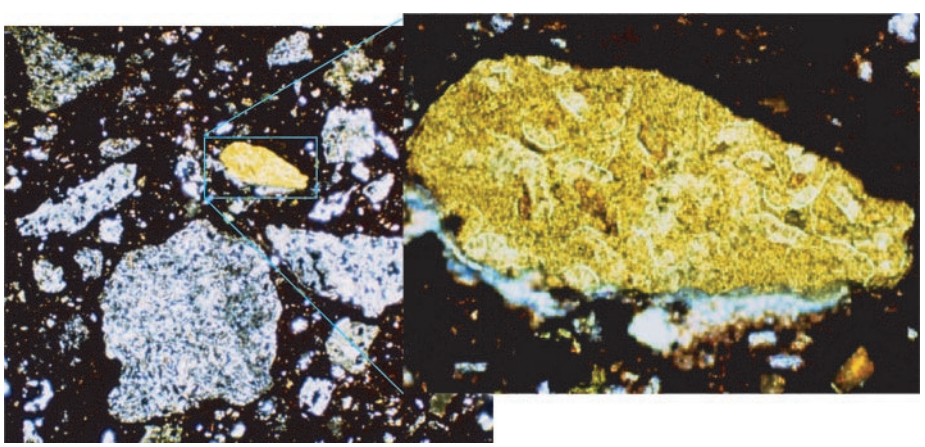

Fig. 5. (**Left**) A typical core sample from the Bedout impact melt breccia at 3052 m (9986 feet) displays a distribution of poorly sorted angular and subangular clasts in a dark glassy matrix (the scale of the picture is 6.5 mm—on the long dimension). (**Right**) Under higher magnification, the yellowish clast appears to be a partially melted carbonate clast with fossil ooids characteristic of a marine continental (carbonate reef) margin environment.

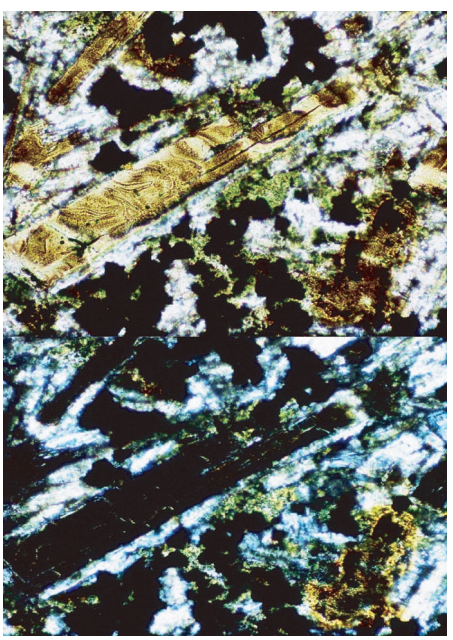

Fig. 6. (**Top**) Photomicrograph taken in plane-polarized light of a sample from Bedout-1 at 3044 m (9986 feet), showing a large plagioclase lath (yellow-brown color indicative of alteration) that has been shock-melted. Another lath at upper left has also been shock-melted (slide width, 550 μm). The shock-melted plagioclase glass is in the process of alteration (green). The matrix is composed of opaque Fe-Ti oxides (black) and albite (clear). (**Bottom**) Same view under crossed nicols. All of the plagioclase laths are now extinct (black) at all orientations, indicating conversion to maskelynite: shock-melted glass that suggests an impact. The two maskelynite laths are at slightly different orientations, yet both are completely extinct.

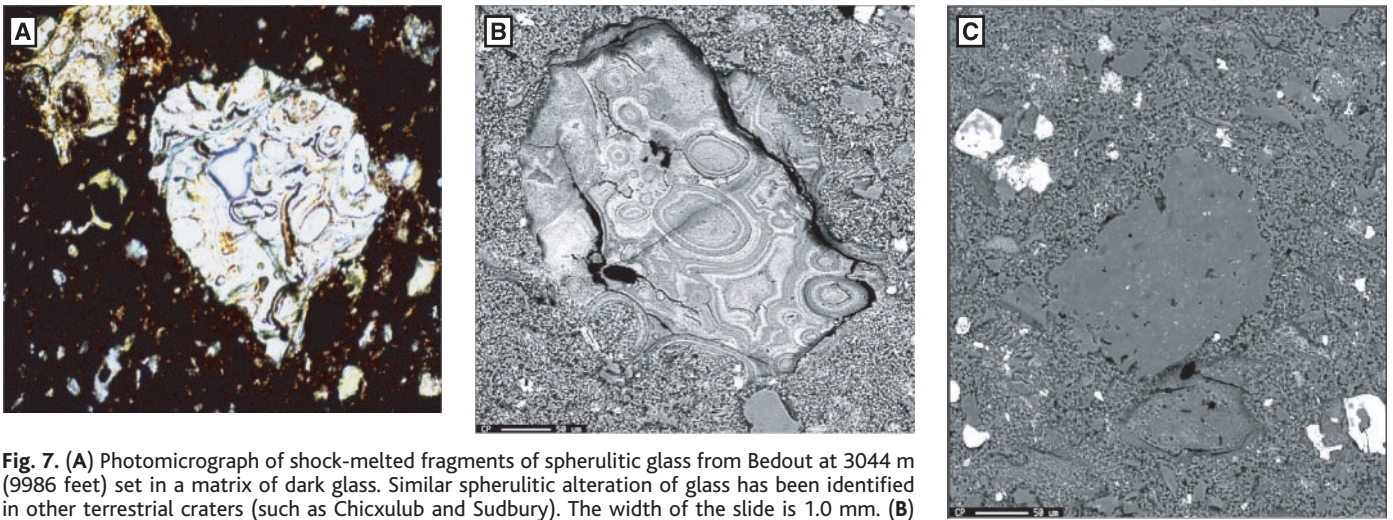

Fig. 7. (**A**) Photomicrograph of shock-melted fragments of spherulitic glass from Bedout at 3044 m (9986 feet) set in a matrix of dark glass. Similar spherulitic alteration of glass has been identified in other terrestrial craters (such as Chicxulub and Sudbury). The width of the slide is 1.0 mm. (**B**) Backscattered electron (BSE) image of another spherulitic glass fragment from Bedout at 3044 m (9986 feet) (table S1, analysis 22). Similar textures have been observed in BSE images of the Chicxulub suevite. Scale bar, 50 μm. (**C**) BSE image of high-silica glass from Bedout at 3044 m (9986 feet). The large grain of nearly pure silica (table S1, analyses 22 and 24) in the center of the image is set in a matrix of plagioclase, altered glass, and Fe-Ti oxides. The dark and light areas of the BSE image correspond to different levels of impurities in the silica glass. Ordinary volcanic processes cannot produce glass of >85% silica. Scale bar, 50 μm.

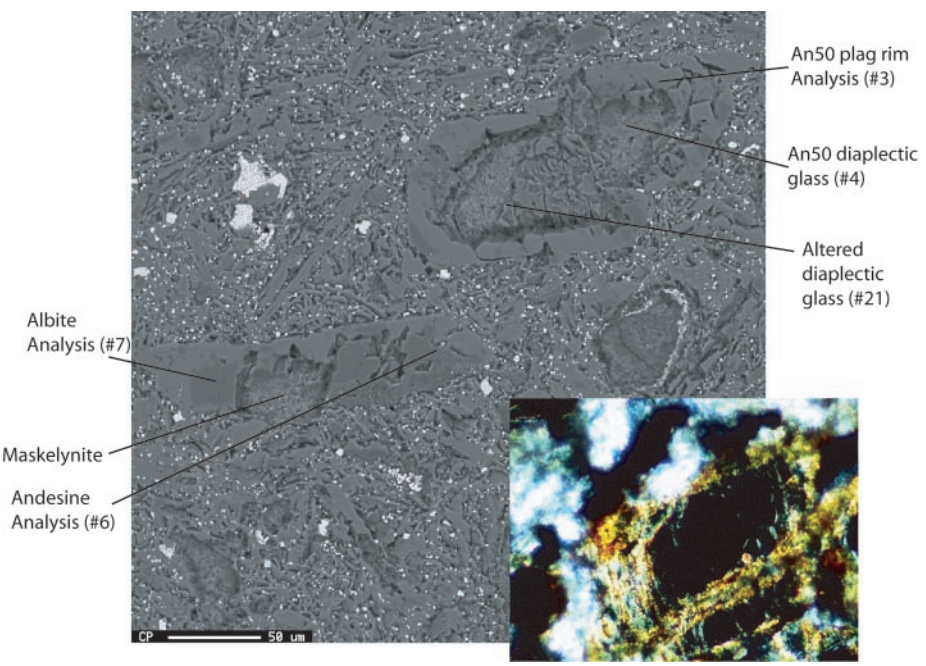

Fig. 8. Shock-melted plagioclase grains from Bedout at 3044 m (9986 feet) set in a matrix of albite, Fe-Ti oxides, and glass that is altering to chlorite. The rim of the large grain in the upper right is crystalline plagioclase (visible in crossed nicols in figure inset) with a composition of An_{50} (analysis 3 in table S1). The core of this grain is isotropic glass with a similar composition of An_{50} plagioclase (analysis 4 in table S1). A single plagioclase lath (left of center) contains andesine plagioclase (An_{50}) (right side of grain, point 6), diaplectic glass in the center, and pure albite (point 7) on the left.

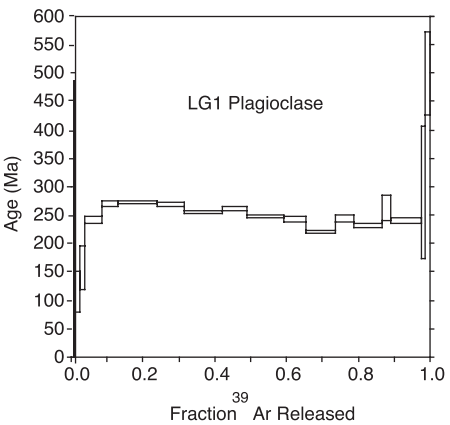

Fig. 9. Ar/Ar step-heating ages for a Lagrange-1 plagioclase separate from 3255 m (10,679 feet) from the top of the Bedout High indicate an age of 250.1 ± 4.5 My.

and glasses of the Bedout core are consistent with a heterolithic impact breccia or melt-rich suevite, formed by impact-triggered heterogeneous melt formation and subsequent quenching and crystallization. Such compositions are unknown and unlikely to exist in terrestrial volcanic agglomerates, lava flows, and intrusive pipes. Individually, some of these minerals may rarely occur in volcanic or plutonic rocks, but never in association with each other.

In particular, natural volcanic processes generate silicate melts up to but not exceeding about 78% silica. Taken as a whole, these features are most consistent with impact-generated melting. Volcanism associated with rifting does not produce melts (glasses) such as nos. 23 and 24 in table S1 (nor does any other endogenous magmatic process). The overall textures of these heterolithic fragments, especially the Bedout glasses, are similar to the features of the Sudbury Onaping breccia and the melt breccias inside the Chicxulub crater (Fig. 4) (*22–24, 28*).

Ar/Ar dating of the Bedout core. We undertook $^{40}Ar/^{39}Ar$ age measurements on feldspar concentrates from the Bedout-1 core and Lagrange-1 impact breccia by step-heating and single-crystal fusion experiments [(*29*) and supporting online material (SOM)]. $^{40}Ar/^{39}Ar$ dates on six individual plagioclases from 3041 m (9977 feet) from the Bedout-1 core indicate ages that are much younger than the overlying Triassic sediments. Petrographic and microprobe examination of the Bedout core from 3044 and 3041 m (9986 and 9977 feet) revealed significant alteration in plagioclase grains and possibly extensive K addition (Figs. 6 to 8 and figs. S8 and S9), resulting in young $^{40}Ar/^{39}Ar$ ages. Individual feldspar grains display heterogeneous chemical compositions due to alteration or disequilibrium in the sample cuttings (table S1 and

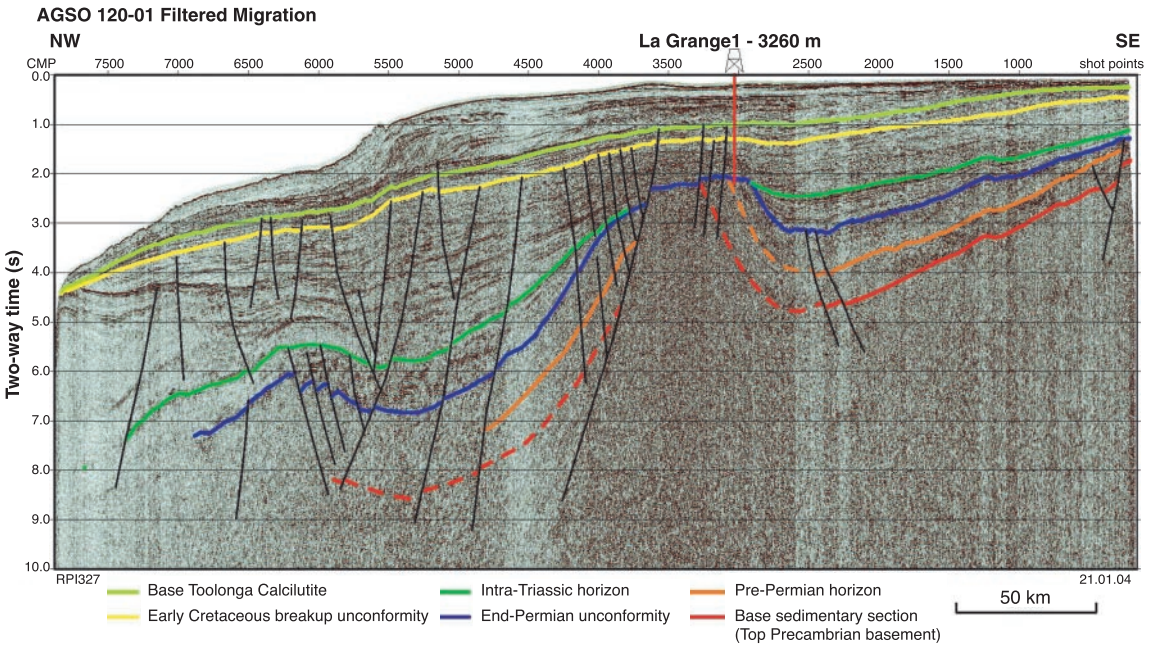

Fig. 10. Reinterpreted 1994 AGSO multichannel seismic line s120-01. This interpretation shows the central uplift of the inferred Bedout impact structure deforming end-Permian (dark blue line) and older sequences (pre-Permian, orange dashed line, and top Precambrian basement, red dashed line), overprinted by younger faults associated with late-Triassic to mid-Jurassic rifting. The "pre-Permian strata" are inferred only from seismic character (*16*), yet appear to show uplift with the basement. These reflectors are carried from wells in the adjacent onshore Canning basin.

fig. S7, A and B). The glassy matrix from 3044 m (9986 feet) had extremely low K (<0.1%) and proved unsuitable for $^{40}Ar/^{39}Ar$ dating. A plagioclase separate at 3255 m (10,679 feet) from the Lagrange-1 cuttings, which displayed the least evidence of alteration or disequilibrium, has an $^{40}Ar/^{39}Ar$ age of 250.2 million years (My), with a plateau portion between 8 and 90% gas release at 250.1 ± 4.5 million years ago (1σ ± 1%), consistent with the previous K-Ar measurement on a plagioclase separate from Lagrange-1 [253 ± 5 My (*30*)] (Fig. 9 and SOM). Similar problems in dating plagioclase separates were observed in the Yucatan-6 melt rocks from the Chicxulub crater (*23*).

Geophysical evidence. Confirmation that the Bedout High consists of an impact breccia and melt sheet led us to reinterpret some seismic lines provided by AGSO (*18*), including line S120-01 (Fig. 10), originally interpreted by Gorter (*13*, *14*). Our revised chronostratigraphy for line S120-01 includes the Lagrange-1 and Bedout-1 stratigraphic sections, correlation with adjacent onshore seismic sections and wells (*31*), and the Ar-Ar and K-Ar dating of the melt breccia. The top of the Permian (blue line, Fig. 10) is conformable with the Bedout High, whereas Triassic sediments (light green line, Fig. 10) unconformably onlap onto the structure (Fig. 10 and fig. S15). The revised seismic section shows a broad uplifted core of basement (red line, Fig. 10) 40 to 60 km in diameter elevated a minimum of 6 to 9 km. The "pre-Permian" strata (Fig. 10), inferred only from seismic character correlations (*16*), are not well imaged in the seismic data and yet appear to show uplift with the basement core. Alternatively, because the deeper material has yet to be sampled and dated, these sequences could all be end-Permian crater-fill impact debris. We also detect a slight uplift of Permian and earlier strata at a radius of ~100 km from the center of the Bedout High, but it is not clear that this is a concentric feature. A two-dimensional velocity model derived from ocean-bottom seismometer wide-angle reflection and refraction data collected along the S120-01 line (*32*) reveals a central uplift beneath the Bedout High, with some 6 to 7 km of vertical structural relief on midcrustal isovelocities. Although less well resolved, the data also suggest possible variations in Moho depth beneath Bedout (*33*). It is difficult to assess, however, whether this Moho topography is, like Chicxulub, the result of the dynamic effects of the crater- (and Bedout High–) forming process extending down to the base of the crust (*33*–*35*) or is the result of later rifting of the continental margin.

The Bedout structure was emergent in the Early to Middle Triassic and is probably deeply eroded. Onshore in the Canning Basin, much of the Permian and Early Triassic section is missing: over 0.5 to 1 km of section overall, and as much as 2 km on topographic highs (*36*). We do not know the depth of erosion at Bedout, but it is probable that the unconformity at the top of the Permian represents a missing section. The Lagrange-1 well extends for several hundred meters through the impact melt breccia, but it is uncertain how much more of the High is actual impact melt breccia. The isostatic residual gravity model for the Bedout structure and the Bouguer gravity over Chicxulub both show a semicircular gravity low surrounding the expression for the central peak (Fig. 11). Unfortunately, the resolution of the offshore gravity data is not of sufficient quality to obtain a vertical derivative image, which is generally used to highlight the more subtle gradients, and assist in assessing the geomorphometric parameters, including size, of the Bedout structure. The outer edge of the gravity low has a diameter of ~100 km and is similar in size to the better-resolved Chicxulub gravity low (Fig. 11).

Comparisons of the Bedout structure with other impact structures. As first noted by Gorter (*13*, *14*), the geophysical expression of the Bedout High is similar to the central uplift in other large impact craters. Fracturing and brecciation, caused by the impact of large meteorites with the crust, produce a characteristic negative gravity anomaly surrounding a gravity high, a feature that led to the initial discovery of Chicxulub (*12*). Such an anomaly exists at Bedout (Fig. 11), but it is somewhat obscured by other complex crustal features derived from younger tectonic overprinting (from the Triassic and Jurassic). The gravity high in the center of large terrestrial craters is due to the central uplift elevating denser basement rocks. At Bedout, the gravity high is clearly associated with a structural high. The central uplift at Chicxulub is poorly imaged seismically, consists mostly of ~6 to 7 km of uplift of midcrustal isovelocities, and is ~40 to 60 km in diameter (*33*). These dimensions compare well with the Bedout High, suggesting that Bedout may be about the same size as Chicxulub (~200 km in diameter). The slight uplift noted at a radius of ~100 km at Bedout may be a subtle expression of the outer rim, but this is speculative. If the Bedout High is a central uplift similar to the one at Chicxulub, then the erosion at Bedout could be extensive, because the top of the Chicxulub central uplift lies about 3.5 km below the crater floor (*37*).

The seismic profile across Bedout is similar to one across the 40-km-diameter Mjølnir crater (fig. S16) in the Barents Sea (*38*), except that the Mjølnir central uplift is much smaller (1.5 to 2 km high and 8 km wide). Mjølnir has a central uplift that extends well above the pre-impact

surface (horizon UB, fig. S16) and is apparently the result of differential subsidence in the annular trough around the peak under the load of post-impact sediments (*39*). Permian strata at Bedout are overlain by ~3 to 5 km of sediment, so it is possible that differential subsidence has altered the relief of the Bedout High since its initial formation.

Evidence for a P-T impact in Gondwana. A large impact crater at Bedout is consistent with the global distribution of impact ejecta in the P-T boundary and helps explain apparent anomalies in the observed patterns. Large (>200 μm) impact ejecta fragments have, so far, only been found in the P-T boundary at sites relatively close to Bedout (Fig. 1). Meteorite fragments from the P-T boundary at Graphite Peak in Antarctica range in size from 50 to 400 μm (*8*) (Fig. 1). We have found shocked quartz ranging from 150 to 550 μm in size at Fraser Park, adjacent to the well-known site at Wybung Head in the Sydney Basin (*4*) (Fig. 12 and fig. S1, A and B) and grains up to 250 μm at Graphite Peak, Antarctica (Fig. 1 and fig. S1). The shocked quartz at Fraser Park and Graphite Peak comprises ~1% of the quartz fraction, compared to ~50% at many K-T boundary sites (*40*). Retallack *et al*. (*4*) suggested that such a small amount of shocked quartz in the P-T boundary may indicate a minor impact, but we interpret the low percentage as a product of dilution by reworking of the ejecta in a continental depositional environment. The P-T boundary layer in the Sydney Basin and in Graphite Peak is a claystone breccia 10 to 20 cm thick containing abundant rip-up clasts from the underlying soil (*4*), whereas the shocked quartz–rich distal K-T boundary deposits are composed mostly of ejecta and are <1 cm thick (*41*).

When the maximum grain sizes of shocked quartz from Fraser Park and Graphite Peak are plotted with respect to distance from Bedout, they match well with the maximum sizes for shocked quartz in the K-T boundary and their distance from Chicxulub (Fig. 12). Pope (*42*) demonstrated that the global shocked quartz distribution in the K-T boundary is best explained by dispersal by stratospheric winds and the settling of the particles through the atmosphere. Such a dispersal mechanism is not efficient in latitudinal transport of debris and, therefore, an impact at Bedout would disperse shocked quartz mostly over the Southern Hemisphere. Thus, a large impact at Bedout is consistent with the size of the shocked quartz grains found in Australia and Antarctica and may also explain why such grains are not found further north.

Elsewhere, in China (Meishan) and Japan (Sasayama), Fe-Ni-Si metal nuggets, oxides, and spherules ~30 to 200 μm in size are found in the P-T boundary (*5*, *6*, *8*, *43*). Similar-sized spherules with refractory grains (Mg-Ni-Fe oxides and Si-Ca-Al oxides) from the K-T boundary are attributed to formation in the Chicxulub vapor plume (*44*), and a similar vapor plume origin has been proposed for the P-T spherules (*5*, *8*). These high-energy vapor plume products are dispersed much more widely than the clastic debris (shocked quartz) (*42*), thus the presence of vapor plume condensates in China and Japan without shocked quartz is consistent with an impact at Bedout. The apparent absence of P-T impact ejecta from sites far to the north of Gondwana, in what is today North America, Europe, and most of Asia (formerly the Laurasia supercontinent), may also be a consequence of a far Southern Hemisphere impact at Bedout, but more work is needed to verify this hypothesis.

Discussion. We have presented geochemical, geochronological, biological, and petrological evidence that links the Bedout structure to end-Permian impact deposits worldwide (Fig. 1). The recognition of an impact breccia in the Bedout High emphasizes the difficulties in interpreting old impact structures that are subtle in their expression and do not retain the pristine characteristics of younger, well-preserved craters such as Chicxulub (*12*). Available drill cores have sampled only the upper portion (~22 m of intact core at Bedout-1 and 391 m of cuttings at Lagrange-1) of the impact melt breccia and contain mostly highly shocked materials. The shock pressures recorded in the Bedout core were sufficient to produce maskelynite (*28*) (pressures of 35 to 45 GPa) and silica glass (>45 to 65 GPa). They were too high to preserve planar deformation features in quartz (<35 GPa) but sufficiently high to form stishovite (15 to 40 GPa) and perhaps hexagonal diamond (70 to 140 GPa) (*45*). Thus, other samples from the Bedout High may produce additional evidence of shock (stishovite, coesite, and diamond), assuming that suitable target rocks were present. Similarly, future analyses may isolate pristine mineral grains for radiometric dating and thus better constrain the end-Permian age and its hypothesized association with the P-T boundary. Additional geophysical data, and perhaps coring, are needed to better determine the size of the structure.

The evidence for yet another impact event coincident (within the age uncertainty) with severe flood basalt volcanism raises the question of the relation of such catastrophes to each other and to mass extinction events (*46*). There has been increasing speculation that large bolide impacts have been responsible for processes such as continental flood basalt eruptions and mantle plumes (*47*, *48*). Present models suggest that an impact may induce a volca-

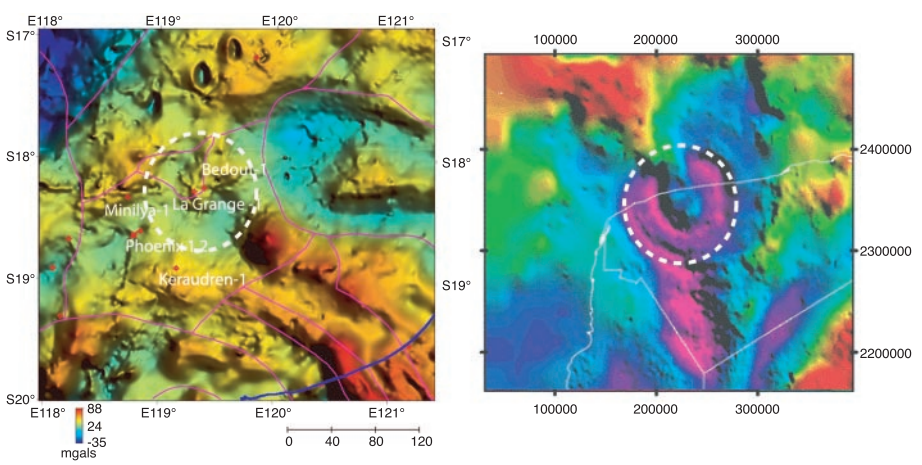

Fig. 11. (Left) Blowup of isostatic residual gravity model over Bedout as compared with **(right)** Bouguer gravity over Chicxulub [modeled after (*12*)] at approximately the same scale. The diameters of the central uplift (~40 to 60 km) and primary collapsed crater (~100 km, dashed circle) inferred from the gravity model for Bedout are similar in size to these same features inferred for the Chicxulub impact structure. The gravity signature at Bedout is significantly reduced and more subdued than at Chicxulub, owing to its greater depth of burial (Bedout gravity model by Andrew Lockwood, GSWA, Perth, Australia).

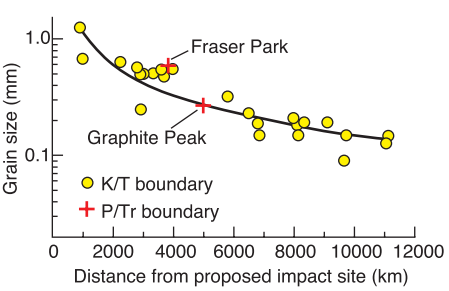

Fig. 12. Shocked quartz in the K-T (yellow circles) and P-T (red crosses) boundaries. Shown is the distribution of the maximum grain size of shocked quartz with distance from the two proposed source craters (Chicxulub for K-T and Bedout for P-T). The solid line is a power regression through the K-T data (*42*).

nic outburst if the bolide strikes a preexisting hot spot. However, the probability of such an event occurring is extremely remote (*49*, *50*). In the case of Chicxulub and now Bedout, the crater locations are opposite (rather than exactly antipodal) (Fig. 1) to the position of the volcanic province (Deccan and Siberia respectively). Indeed, Melosh (*49*) has calculated that the amount of kinetic energy needed to create the volume of the Deccan traps (~500,000 km^3) would require some 5×10^{23} J or twice the amount of kinetic energy generated by the Chicxulub impactor (10 km at 20 km/s).

Although it seems clear that an impact may not be the direct cause of the volume of flood basalts, it may still act as a "trigger" of the event. At both Siberia and Deccan, Ar-Ar dating has shown that volcanic rocks with mantle plume affinities predate the main pulse of the Deccan and Siberian traps (*51*, *52*). Thus, the impact(s) and subsequent energy release might enhance the catastrophic eruption of a preexisting mantle plume. New models may need to be considered to properly assess, identify, and confirm extraterrestrial impact events and to further understand the impact process and its relation to severe volcanism and mass extinctions in the geologic record.

References and Notes

1. L. Becker *et al*., *Science* **291**, 1530 (2001).
2. L. Becker, R. J. Poreda, T. E. Bunch, *Proc. Natl. Acad. Sci. U.S.A.* **97**, 2979 (2000).
3. L. Becker, C. Nicholson, R. J. Poreda, *American Geophysical Union (AGU) Abstract*, December 12 to 17 2002, OS22C-0291 (2002).
4. G. J. Retallack *et al*., *Geology* **26**, 979 (1998).
5. K. Kaiho *et al*., *Geology* **29**, 815 (2001).
6. S. Miono, Y. Nakayama, K. Hanamoto, *Nucl. Instrum. Methods Phys. Res. Sect. B Beam Interactions Mater. Atoms* **150**, 516 (1999).
7. R. J. Poreda, L. Becker, *Astrobiology* **3**, 120 (2003).
8. A. R. Basu, M. I. Petaev, R. J. Poreda, S. B. Jacobsen, L. Becker, *Science* **302**, 1388 (2003).
9. Similar metal grains are found in the boundary layer (at the base of bed 25) at Meishan, China (*5*). The common occurrence of Fe-Ni-Si grains at the Graphite Peak, Antarctica, and Meishan, China, P-T boundary layers is evidence for their apparent relationship as pointed out in (*8*). These "event-marker" magnetic grains occur only in the boundary layer and are absent in samples above and below, both at Meishan and Graphite Peak. The unique chemical composition of the metal-rich grains (for example, condensates) suggests formation in the vapor cloud as a result of the impact event (*8*).
10. S. Miono, C. Z. Zheng, Y. Nakayama, *Nucl. Instrum. Methods Phys. Res. Sect. B Beam Interactions Mater. Atoms* **109**, 612 (1996).
11. L. Alvarez, W. Alvarez, F. Asaro, H. Michel, *Science* **208**, 1095 (1980).
12. A. R. Hildebrand *et al*., *Geology* **19**, 867 (1991).
13. J. Gorter, *Pet. Explor. Soc. Aust. News* **1996**, 33 (1996).
14. J. Gorter, *Aust. Pet. Prod. Explor. Assoc. J.* **1998**, 159. (1998).
15. The JNOC data range from very poor to moderate in quality. Most sections are adversely affected by seafloor multiples due to shallow water depth. These lines are now being reprocessed by Seismic Australia to improve the quality of the data and will be incorporated in future studies.
16. S. A. Smith, thesis, University of Adelaide, Adelaide, Australia (1999).
17. P. G. Purcell, R. R. Purcell, in *The Sedimentary Basins of Western Australia*, P. G. Purcell, R. R. Purcell, Eds. [Proceedings of the Petroleum Exploration Society of Australia (PESA) Symposium, PESA, Perth, Australia, 1994], pp. 769–777.
18. AGSO NW Shelf Study Group, in *The Sedimentary Basins of Western Australia*, P. G. Purcell, R. R. Purcell, Eds. (Proceedings of the PESA, Symposium, PESA, Perth, Australia, 1994), pp. 63–76.
19. S. Colwell, B. Stagg, in *The Sedimentary Basins of Western Australia*, Purcell, P. G. Purcell, R. R. Purcell, Eds. (Proceedings of the PESA, Symposium, PESA, Perth, Australia, 1994), pp. 757–768.
20. Well reports, La Grange-1 and Bedout-1 exploration wells [Geological Survey of Western Australia (GSWA), Perth, Australia, 1971 and 1983].
21. T. R. Charlton, *J. Asian Earth Sci.* **19**, 595 (2001).
22. B. C. Schuraytz, V. L. Sharpton, L. E. Marin, *Geology* **22**, 868 (1994).
23. V. L. Sharpton *et al*., *Nature* **359**, 819 (1992).
24. P. Claeys, S. Heuschkel, E. Lounejeva-Baturina, G. Sanchez-Rubio, D. Stoffler, *Meteorit. Planet. Sci.* **38**, 1299 (2003).
25. The Bedout-1 impact melt breccia is similar to the Yucatan-6 (Fig. 4) melt breccia, with centimeter-sized clasts of fine-grained to glassy, typically altered, melt rock in a fine- to medium-grained melt rock matrix composed mainly of feldspars, chlorite, and carbonate. If the Bedout impact melt breccia reflects the compositions of the target rocks, then one can assume that the upper part of the Bedout basement was dominated by more feldspar-rich rocks or basaltic volcanics (*24*). The difference between the Bedout-1 and Yucatan-6 impact melt breccias is that most of the clasts and the matrix in Bedout have been pervasively altered to chlorite.
26. The fossil ooid fragments and carbonate clast lack shock features but are intimately associated with the glassy (silicate) matrix, which is consistent with an impact origin. Similar observations have been made for the Haughton, Ries, and Chicxulub crater breccias. These textural features may be attributed to carbonate-silicate liquid immiscibility (*27*). The recognition of fossil ooids in the end-Permian–aged Bedout-1 impact melt breccia suggests that sedimentary (marine) target rocks were also present at the time of impact.
27. G. Graup, *Meteorit. Planet. Sci.* **34**, 425 (1999).
28. B. M. French, *Traces of Catastrophe: A Handbook of Shock-Metamorphic Effects in Terrestrial Meteorite Impact Structures* (LPI Contribution No. 594, Lunar Planetary Institute, Houston, TX, 1998).
29. We used the biotite standard GA1550, developed at the Australian National University Research School of Earth Sciences (RSES) in Canberra, Australia, the in-house standard for the past 35 years that is now widely recognized as one of the best primary (meaning fundamentally calibrated) standards in the world. For the purpose of this study, the 98.5 My (biotite) standard age was used, which is good to better than 0.3% for determining the J-value neutron flux parameter of irradiation. All materials were inspected under a binocular microscope before irradiation. Notable brown staining discolored most of the grains and is likely due to iron oxides. The concentrates were weighed and wrapped in aluminum foil. Samples were then sealed in an outer aluminum canister. The inner packaging components consisted of a pure silica glass tube with a cadmium liner (0.2 mm thick) between the glass and outer canister. The fluence monitor biotite GA1550 (K/Ar age of 98.5 ± 0.8 My) was packed in the canister at regular intervals. The canister was then irradiated for 4 days in the Heavy Ion Fusion Accelerator Reactor (HIFAR) reactor at Lucas Heights, New South Wales. The canister was inverted three times during the irradiation, to reduce the neutron fluence gradient across the container. After irradiation and a cooling-off period, samples and standards were repacked in aluminum foil. The biotite standard and plagioclase unknowns were loaded onto an extraction line connected to a VG 3600 gas source mass spectrometer with a resolution of ~600. Samples were heated in a series of steps, with each sample subjected to approximately 15 steps, for a duration of 14 min for each step. Data were reduced using the Macintosh program Noble, developed at the RSES, Canberra, Australia. Correction factors to account for K-, Cl-, and Ca-derived Ar isotopes are $(^{36}Ar/^{37}Ar)Ca = 3.5 \times 10^{-4}$, $(^{39}Ar/^{37}Ar)Ca = 7.86 \times 10^{-4}$, $(^{40}Ar/^{39}Ar)K = 2.2 \times 10^{-2}$, $(^{38}Ar/^{39}Ar)K = 0.136$, and $(^{38}Ar)Cl/(^{39}Ar)K = 8.0$. Blanks and backgrounds were generally atmospheric and/or insignificant in terms of fraction of gas analyzed. Air standards were used to determine mass fractionation, which is known within about 0.3% and was assumed not to vary on the time scale of sample analysis.
30. Sample cuttings from the Lagrange-1 well (latitude 18°16′37.4′′S, longitude 119°18′0.7.2′′E) were provided by the British Petroleum Company (BP) to A. Webb of Amdel Petrology, Australia. The results were published in the BP company report (*20*) and are currently available upon request from Geoscience Australia in Canberra or the GSWA. K/Ar dating was performed on plagioclases handpicked by Webb from cuttings sampled in the lowest (10,215 feet) section of the Lagrange-1 exploration well. This sample was described as suitable for age dating, resulting in an age of 253 ± 5 My.
31. S. A. Reechmann, A. J. Mebersen, in P. G. Purcell, Ed., *The Canning Basin, Western Australia* [Proceedings of the Geological Society of Australia/PESA (GSA/PESA) Canning Basin Symposium, PESA, Perth, Australia, 1984], pp. 389–400.
32. A. Kritski, thesis, University of Sydney, Sydney, Australia (2000).
33. G. L. Christeson, Y. Nakamura, R. T. Buffler, J. Morgan, M. Warner, *J. Geophys. Res.* **106**, 751 (2001).
34. J. Melosh, *Nature* **414**, 861 (2001).
35. Like Chicxulub, the refraction data show that the Moho is distorted beneath the Bedout High (*33*, *34*). The rise of the Moho, however, is slightly offset from the central peak, suggesting that the material beneath the transient crater (~20 km of crust) was not just simply pushed down under the crater floor as observed for Chicxulub (*34*). The deeper crustal structure of Bedout is less well resolved (*32*); thus, its relation to the Bedout High and subsequent continental rifting needs further investigation.
36. E. L. Horstman, in *The Canning Basin, Western Australia*, P. G. Purcell, Ed. (Proceedings of the GSA/PESA Canning Basin Symposium, PESA, Perth, Australia, 1984), pp. 240–267.
37. J. Morgan, M. Warner, *Geology* **27**, 407 (1999).
38. F. Tsikalas, S. T. Gudlaugsson, J. I. Faleide, *J. Geophys. Res.* **103**, 30, 430 (1998).
39. F. Tsikalas, S. T. Gudlaugsson, J. I. Faleide, *Geol. Soc. Am. Bull.* **110**, 537 (1998).
40. G. A. Izett, *Geol. Soc. Am. Spec. Pap.* **249**, 100 (1990).
41. J. Smit, *Annu. Rev. Earth Planet. Sci.* **27**, 75 (1999).
42. K. O. Pope, *Geology* **30**, 99 (2002).
43. M. I. Petaev, S. B. Jacobsen, A. R. Basu, L. Becker, *Lunar Planet. Sci. Conf. Abstr.* **XXXV**, 1216 (2004).
44. F. T. Kyte J. A. Bostwick, *Earth Planet. Sci. Lett.* **132**, 113 (1995).
45. D. Stöffler, *Fortschr. Mineral.* **49**, 50 (1972).
46. M. K. Riechow *et al*., *Science* **296**, 1846 (2002).
47. A. P. Jones *et al*., *Earth Planet. Sci. Lett.* **6343**, 1 (2002).
48. A. Glikson, *Geology* **27**, 387 (1999).
49. H. J. Melosh, Catastrophic Events and Mass Extinction: Impacts and Beyond Conference Abstract 3144 (2000).
50. B. A. Ivanov, H. J. Melosh, *Lunar Planet. Sci. Conf. Abstr.* **XXXIV**, 1338 (2003).
51. P. R. Renne, A. R. Basu, *Science* **253**, 176 (1991).
52. A. R. Basu *et al*., *Science* **261**, 902 (1993).

53. Supported by NASA grants in Exobiology and by an NSF Continental Dynamics Workshop sponsored by L. Johnson. We thank P. Cronin and E. Resiak for assistance with the Bedout-1 and Lagrange-1 core sampling and A. Fleming for access to the AGSO regional seismic survey. We also thank the GSWA in Perth for hosting the NSF workshop and R. Emms

and A. Mory for assistance with additional core sampling and access to well reports. Special thanks go to J. Hunt for assistance with the microprobe; AINSIE and ANSTO for the neutron irradiation of the Bedout core material and funding; A. Lockwood for the Bedout High gravity model; J. Dunlap for assistance with the argon dating; F. Tsikalas for use of the Mjølnir figure; A. Kritski and S. Smith for access to their thesis data; and G. Retallack, A. Glikson, J. Gorter, and the Bedout Working Group for many helpful discussions and suggestions.

Supporting Online Material
www.sciencemag.org/cgi/content/full/1093925/DC1

Figs. S1 to S19
Tables S1 to S3

20 November 2003; accepted 28 April 2004
Published online 13 May 2004;
10.1126/science.1093925
Include this information when citing this paper.

REPORTS

Toward Heisenberg-Limited Spectroscopy with Multiparticle Entangled States

D. Leibfried,* M. D. Barrett,† T. Schaetz, J. Britton, J. Chiaverini, W. M. Itano, J. D. Jost, C. Langer, D. J. Wineland

The precision in spectroscopy of any quantum system is fundamentally limited by the Heisenberg uncertainty relation for energy and time. For *N* systems, this limit requires that they be in a quantum-mechanically entangled state. We describe a scalable method of spectroscopy that can potentially take full advantage of entanglement to reach the Heisenberg limit and has the practical advantage that the spectroscopic information is transferred to states with optimal protection against readout noise. We demonstrate our method experimentally with three beryllium ions. The spectroscopic sensitivity attained is 1.45(2) times as high as that of a perfect experiment with three nonentangled particles.

Quantum-mechanical entanglement in an ensemble of particles can enhance the signal-to-noise ratio in spectroscopy to a level that is fundamentally unattainable with non-entangled particles. The enhancement is ultimately limited by the Heisenberg uncertainty relation between energy and time. Experiments that approach the Heisenberg limit have been rare because of the difficulty of producing suitable entangled states and because of the lack of robust observables that realize the limit for a large number of particles when the intermediate operations and the readout of the final state are imperfect. The method described here relies solely on collective interactions without the need to individually address the particles, and the final observable is the global state population of the ensemble. Therefore, neither exact knowledge of the number of particles in the ensemble nor individual particle access in preparation or readout is required to reach the Heisenberg limit.

A transition between any two quantum states is formally equivalent to a transition between the two states of a spin-$\frac{1}{2}$ system. We will label the eigenstates of the z-component of spin $\tilde{S}_z$ as $|\downarrow\rangle$ and $|\uparrow\rangle$ with $\tilde{S}_z|\downarrow\rangle = -\frac{1}{2}|\downarrow\rangle$ and $\tilde{S}_z|\uparrow\rangle = \frac{1}{2}|\uparrow\rangle$, where we choose units such that $\hbar = 1$ and assume that spectroscopy is performed on an ensemble of N such systems with the use of Ramsey interferometry (*1*). For each experiment, the spins are initialized to the state $|\downarrow, N\rangle \equiv |\downarrow\rangle_1|\downarrow\rangle_2 \cdots |\downarrow\rangle_N = |J = N/2, J_z = -N/2\rangle$, where the last expression is written in terms of the N-spin Bloch vector representation, where $\vec{J} = \sum_{i=1}^{N}\vec{S}_i$. The first Ramsey pulse and free precession for duration T produces a state (in a rotating reference frame) that contains phase factors $\phi = (\omega - \omega_0)T$, where ω characterizes the frequency of the applied field and ω_0 is the resonant transition frequency between states $|\downarrow\rangle$ and $|\uparrow\rangle$. The second Ramsey pulse renders the phase information accessible in a global-state observable.

In traditional Ramsey spectroscopy with unentangled atoms (*1*), both pulses implement a rotation $\tilde{R}_x \equiv \exp[i\frac{\pi}{2}\tilde{J}_x]$ (a "$\pi/2$ pulse"). The readout determines the number of atoms $\tilde{N}_\downarrow = N/2 - \tilde{J}_z$ in the $|\downarrow\rangle$ state, where $\langle\tilde{J}_z\rangle = \frac{N}{2}\cos[(\omega - \omega_0)T]$. The final uncertainty $\Delta(J_z)_{\text{final}}$ in $\langle\tilde{J}_z\rangle$ yields a corresponding phase uncertainty

$$\Delta\phi = \Delta\{(\omega - \omega_0)T\} = 1/\sqrt{N} \quad (1)$$

which can be termed the standard quantum limit (*2*, *3*). Any method is ultimately limited to a phase uncertainty of $\Delta\phi = 1/N$, usually called the Heisenberg limit (*4*, *5*).

One way to increase phase sensitivity over Eq. 1 is through "spin squeezing" (*6*–*14*). Such squeezing can, for example, be realized by transferring squeezing from a mechanical (*3*, *7*) or field (*9*, *11*) mode to the spins. It has been shown that the initial spin state $|\downarrow, N\rangle$ could be squeezed by an interaction of the form $U_{\text{sqz}} = \exp[i\chi\tilde{J}_x^2]$ with a suitable coupling parameter χ (*8*). This operator can be implemented in atomic systems (*10*, *12*), and it was demonstrated experimentally on two spins (*13*). It can also be implemented with rotations and phase gates (*12*, *15*, *16*). Spin squeezing has also been realized recently in the context of quantum nondemolition measurements (*14*).

The above methods rely on measuring the orientation of the Bloch vector $\vec{J}$; however, other input states and measurements can also be used, such as initial states of the form $|J = N/2, J_z = 0\rangle$ and a variance measurement operator $\tilde{J}_z^2 - \langle\tilde{J}_z\rangle^2$ (*17*, *18*). Another method (*5*) uses an N-particle Greenberger Horne Zeilinger (GHZ) state (*19*, *20*)

$$\Psi_{\text{GHZ}} \equiv \frac{1}{\sqrt{2}}(|\downarrow, N\rangle + e^{i\zeta}|\uparrow, N\rangle)$$

produced by a "generalized Ramsey pulse," where $|\uparrow, N\rangle \equiv |J = N/2, J_z = +N/2\rangle$ and ζ is a phase factor. After free precession, the final pulse is a rotation $\tilde{R}_x$, applied to all particles, and the measured observable is the parity $\tilde{\Pi} \equiv \Pi_{i=1}^{N} 2(\tilde{S}_z)_i$. This protocol can reach the Heisenberg limit for any value of $(\omega - \omega_0)T$, but has the disadvantage that measurement of the parity is very difficult for large values of N because it requires the ability to distinguish between odd and even numbers of particles in $|\downarrow\rangle$ in the presence of noise. Both protocols have been demonstrated experimentally on two spins (*13*).

The method described here combines ideas from precision spectroscopy and quantum information processing. The goal is to first encode a fiducial initial state into a state

National Institute of Standards and Technology, 325 Broadway, Boulder, CO 80305, USA.

*To whom correspondence should be addressed. E-mail: dil@boulder.nist.gov

†Present address: Department of Physics, University of Otago, Post Office Box 56, Dunedin, New Zealand.